International Communications in Heat and Mass Transfer 136 (2022) 106182

Contents lists available at ScienceDirect

International Communications in Heat and Mass Transfer

journal homepage: www.elsevier.com/locate/ichmt

Exploring thermal contact conductance between two contact solids by artificial neural network

Xing-Jie Ren [a,b], Jian-Jun Gou [c], Yan-Jun Dai [a], Wen-Quan Tao [a,*]

[a] Key Laboratory of Thermo-Fluid Science and Engineering of MOE, School of Energy and Power Engineering, Xi'an Jiaotong University, Xi'an, Shaanxi 710049, China
[b] Institute of Advanced Technology, Shandong University, Jinan, Shandong 250100, China
[c] Shaanxi Aerospace Flight Vehicle Key Laboratory, School of Astronautics, Northwestern Polytechnical University, Xi'an, Shaanxi 710072, China

ARTICLE INFO

Keywords:
Thermal contact conductance
Artificial neural network
Steady-state measurement
Thermal conductivity prediction

ABSTRACT

Realizing accurate measurement for thermal contact conductance (TCC) is difficult and needs many additional measurements. In this paper, we design a three-layer back propagation artificial neural network (ANN) model to retrieve TCC of two contact solid specimens. The model can retrieve TCC only according to the measured temperatures and loading pressures, and the effects of loading pressure, temperature and surface roughness on TCC are considered. Besides, thermal conductivity, heat flux and the parameter of the TCC empirical fitting formula can be obtained simultaneously. The retrieved results are validated by experimental values. The results show that for two contact pairs with different surface roughness, the retrieved parameters of TCC empirical fitting formula are clear reasonable and can be explained conceptually compared with the published studies.

1. Introduction

All seemingly smooth surfaces are actually rough, which can result in an imperfect and discrete contact when two solid surfaces contact each other. Thus, a temperature difference will occur at the interface when heat flows through the interface, and such a phenomenon is entitled as thermal contact resistance (TCR). The reciprocal of TCR is thermal contact conductance (TCC). TCC is defined in the equation $h = q/\Delta T$, where q is the heat flux through the interface and ΔT is the temperature difference at the interface.

TCC can be a crucial influencing factor in the process of heat transfer between two solid surfaces and has a remarkable effect on accurate thermal management in many engineering applications. For example, it can affect the performance of temperature protection system (TPS) of the hyper sonic vehicles [1]. In addition, TCR accounts for more than 50% of the total thermal resistance in press-pack insulated gate bipolar transistor (PP-IGBT) device, thus, it can affect the heat dissipation of the device and lead to a high junction temperature [2]. Besides, the fields of superconducting [3], cryogenic [4], fuel cell [5], fin-tube exchangers [6] should also consider the effect of TCC on the performance of heat dissipation.

TCC can be influenced by surface topography [7], loading pressure [8], temperature [9], the medium trapped in the interface gap [10,11], etc., so it is difficult to obtain a universally valid theory to determine TCC. Although the analytical studies on TCC have been conducted for a long time [12,13], some bottlenecks haven't been broken yet and further studies in rough surface characterization and the asperity deformation of the interface are still necessary. Nowadays, researchers tend to use numerical simulations and experimental methods to determine TCC of the specific materials, besides, using machine learning method to retrieve TCC is a new approach in recent years.

In numerical simulation for TCC, the reconstruction of the rough surface is one of the main difficulties, thus we can divide the numerical simulation for TCC into two main categories according to the published studies. One uses assumptive functions to generate rough surfaces [14–17]. Rather than using assumptive functions, the other uses high-resolution microscope to measure the surface topography of the specimens, and the measured data are used to regenerate the rough surfaces [18–20]. Generally, the model reconstructed from the measurement data is more accurate than the model based on the assumptive rough surfaces [21].

In terms of experimental methods, based on the ASTM E1225–13 standard [22], one dimensional steady-state heat flux method is the most conventional measurement method for TCC. For this experimental setup, after obtaining the temperature distribution of the specimens, the extrapolation method [23] and the linear fitting method [9] are two main methods to calculate TCC. However, the first method needs to

* Corresponding author.
E-mail address: wqtao@mail.xjtu.edu.cn (W.-Q. Tao).

https://doi.org/10.1016/j.icheatmasstransfer.2022.106182

Available online 14 June 2022

Nomenclature

c_1,c_2, c_3	Parameter of empirical fitting formula of TCC $^{--}$
E	Elastic modulus (GPa)
h	Thermal contact conductance ($W{\cdot}K^{-1}{\cdot}m^{-2}$)
P	Loading pressure (MPa)
q	Heat flux ($W{\cdot}m^{-2}$)
R	Thermal contact resistance ($K{\cdot}m^2{\cdot}W^{-1}$)
Ra	Average surface roughness (μm)
T	Temperature (°C)
T_{ave}	Interface average temperature (°C)
x, y, z	Cartesian coordinates (m)
λ	Thermal conductivity ($W{\cdot}m^{-1}{\cdot}K^{-1}$)

measure the thermal conductivity of the specimens before the temperature distribution measurement of the specimens. The second method needs to use additional heat flux meter bars; besides, the thermal conductivity of the specimens should be nearly constant within a not large variation range of temperature. In addition, it should be noted that for the same experimental data, the results derived from these two methods may be obviously different, because this experimental setup is an indirect measurement method, and the measurement error will be enlarged step by step when calculating the temperature difference and heat flux of the interface [24–26].

Actually, solving TCC is an inverse problem of heat transfer, hence, researchers try to apply artificial neural network (ANN) model to solve TCC in recent years. ANN model is an effective method for finding the relations between dependent and independent variables for which mathematical formulation is unavailable. Goudarzi [27] studied the TCC in the exhaust valve of internal combustion engine with an ANN model, in their research, the training data was obtained by solving the inverse problem, and the simulated temperature was used, furthermore, thermal conductivities of the materials should be known and was a constant. Zhan et al. [28] collected the published 876 experimental data of thermal boundary resistance (TBR) to train the model, however, the collected experimental data should be carefully selected because those data were obtained based on different descriptors, such as thermal conductivity, Debye temperature, speed of sound, elastic modulus, and bulk modulus, etc. Yang et al. [29] used the numerical results by classical molecular dynamics (MD) to train the ANN model and predict the TBR between graphene and hexagonal boron-nitride, nevertheless, MD is time-consuming and needs much computational resource. On the other hand, the methods published in [28,29] are difficult to extend to macroscopic TCC prediction.

In this paper, we try to fill this gap by using an artificial neural network (ANN) model to retrieve TCC directly. The model doesn't need to measure the thermal conductivity of the specimens or use heat flux meter bars, on the contrary, the thermal conductivity and heat flux of the specimens can also be retrieved simultaneously only according to the measured temperatures and pressures. The training data can be obtained by a theoretical analysis, and the model is time-saving and whole retrieving process just takes several minutes in a personal computer. Moreover, the model is also useful for contact pairs with different surface roughness.

2. Temperature and pressure measurement

2.1. Experimental apparatus

The measurement schematic for TCC is shown in Fig.1. TCC is derived from the measured temperature distribution of the specimens. Generally, temperatures are measured by thermocouples embedded in the specimens, while IR camera can be also used to measure the temperature difference of the interface [30]. In this study, we use thermocouples to measure temperature distributions.

The measurement apparatus in this study are shown in Fig.2. It should be emphasized that the surface topography of the specimens should be measured firstly before the TCC measurement. The microscope shown in Fig.2 (a) can measure surface topography by optical interference principle. It can accurately measure many parameters of surface topography of and we finally select the conventional average surface roughness, denoted by *Ra*, to represent the surface roughness. The temperature distribution can be measured by a temperature distribution measurement system shown in Fig.2 (b). The system can record loading pressures and steady-state temperatures of two specimens. The more detailed information about these two apparatus can be found in [9].

2.2. Specimens

Fig.3 shows the specimens. The sizes of all specimens are identical, and each cylindrical specimen is 48 mm in diameter and 52 mm in height. Each specimen has 12 holes to mount thermocouples, and every

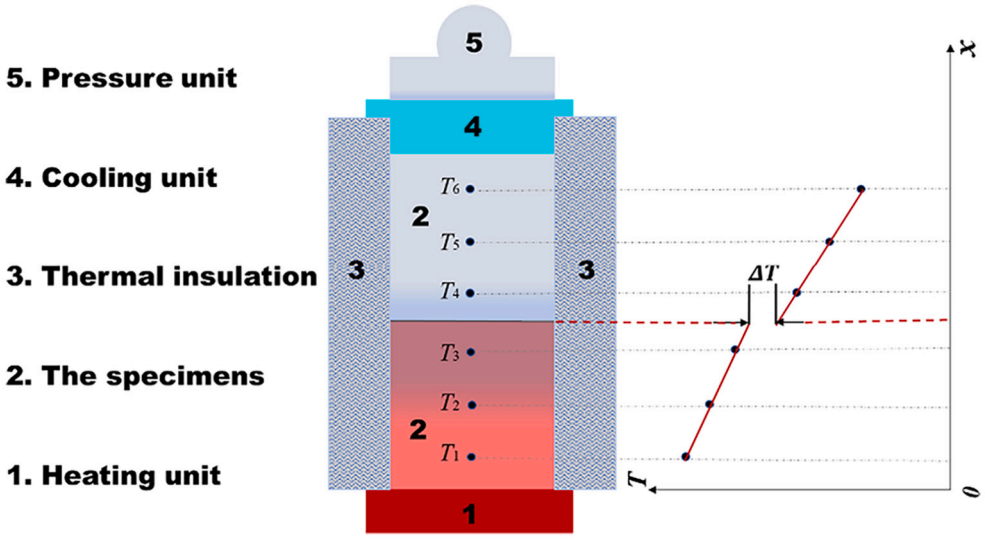

Fig. 1. The schematic of measurement for TCC.

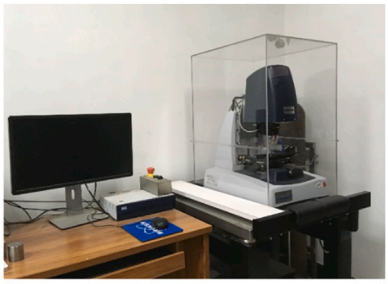

(a) Surface topography measurement system

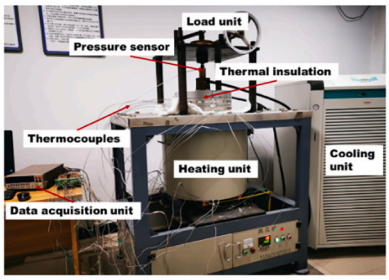

(b) The measurement system of temperature and loading pressure

Fig. 2. The measurement apparatus.

four holes are in the same height and uniformly distributed in the peripheral direction. Every hole is 2 mm in diameter and 12 mm in depth. The sheathed thermocouples with 2 mm in diameter are inserted in the holes to measure the temperatures.

The materials of Pair A (Fig.3(a)) and Pair B (Fig.3(b)) are both TC4 titanium alloy, and the only difference is their surface roughness of two contact surfaces. The two surfaces brought into contact of Pair A are processed by turning and the two surfaces brought into contact of Pair B are processed by sandblasting method. The detailed surface roughness brought into contact measured by the microscope (Fig.2 (a)) is listed in Table 1.

The next step is to measure the temperature distribution of two pairs under different loading pressures and temperatures, which can be finished in the temperature distribution measurement system (Fig.2 (b)). The experimental cases are listed in Table 2. The measurement process can be described as follows. Firstly, fix the pressure at 4.65 MPa, and set the heating temperature to 400 °C , when finish the steady-state temperature record at 400 °C, then increase the temperature to 500 °C and record the steady-state temperature at 500 °C, until finish the measurement under 700 °C. Secondly, increase the pressure to 7.78 MPa, and record the steady-state temperature at different heating temperatures. Lastly, finish the steady-state temperature measurement at 12.08 MPa. In this study, the criteria to judge steady state is that temperature change is less than 0.3 °C with 30 min.

Rather than using the method mentioned in [9,23] to obtain TCC, in this paper, we design an ANN model to retrieve TCC, thermal conductivity and heat flux of the specimens. Although the material of the specimens is TC4 titanium alloy and its thermal conductivity can be found in published data, we still assume the thermal conductivity are unknown in the retrieving process, thus, we can use TC4 titanium alloy to validate our model. The detailed process is described in Section 3.

3. ANN method

3.1. A brief introduction of ANN

In the conventional programming, we tell a computer to break a big problem up into many small and precisely defined tasks that can be easily be performed. By contrast, in ANN we don't tell the computer how to solve our problem. Instead, it learns from training data and figures out its own solution to the problem [31].

A conventional ANN consists of an input layer, one or more hidden layers and an output layer, and each layer has one or more neurons. If the output from one layer is used as input to the next layer, such networks are called feedforward neural networks. Each neuron has a weight and bias, and the data are transferred by the activation function to next neuron. Training algorithm is one of the key parts in an ANN, nowadays, the error backpropagation (BP) algorithm is often used to train ANN. Generally, an ANN with 1 hidden layer can solve most of complicated non-linear problems.

3.2. Theoretical analysis

In this part, we want to discuss how we apply an ANN model to retrieve TCC between two contact solids. As Fig.4 (a) shows, two cylindrical solid specimens contact each other.

Table 1
Surface roughness of two contact pairs.

Contact pair	Surface roughness (*Ra*)
Pair A	2.85 μm / 3.13 μm
Pair B	24.46 μm / 13.36 μm

Table 2
Experimental cases.

Pressure	4.65 MPa	7.78 MPa	12.08 MPa
Heating Temperature	400 °C	400 °C	400 °C
	500 °C	500 °C	500 °C
	600 °C	600 °C	600 °C
	700 °C	700 °C	700 °C

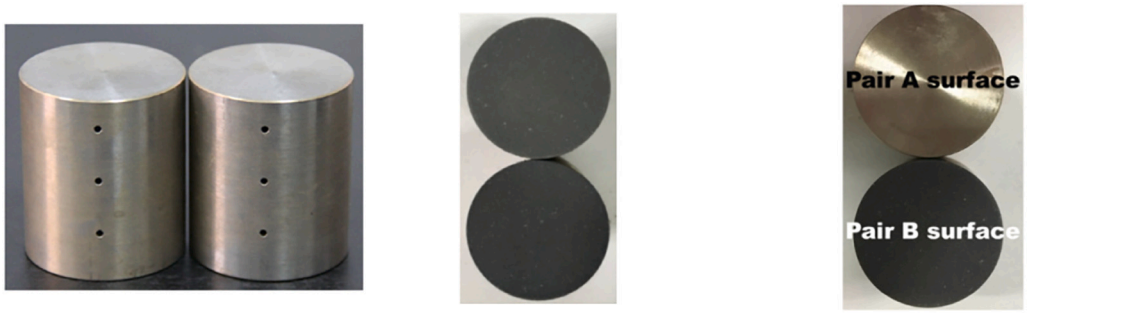

(a) Pair A (b) Pair B (top view) (c) Surfaces of Pair A and Pair B

Fig. 3. The specimens.

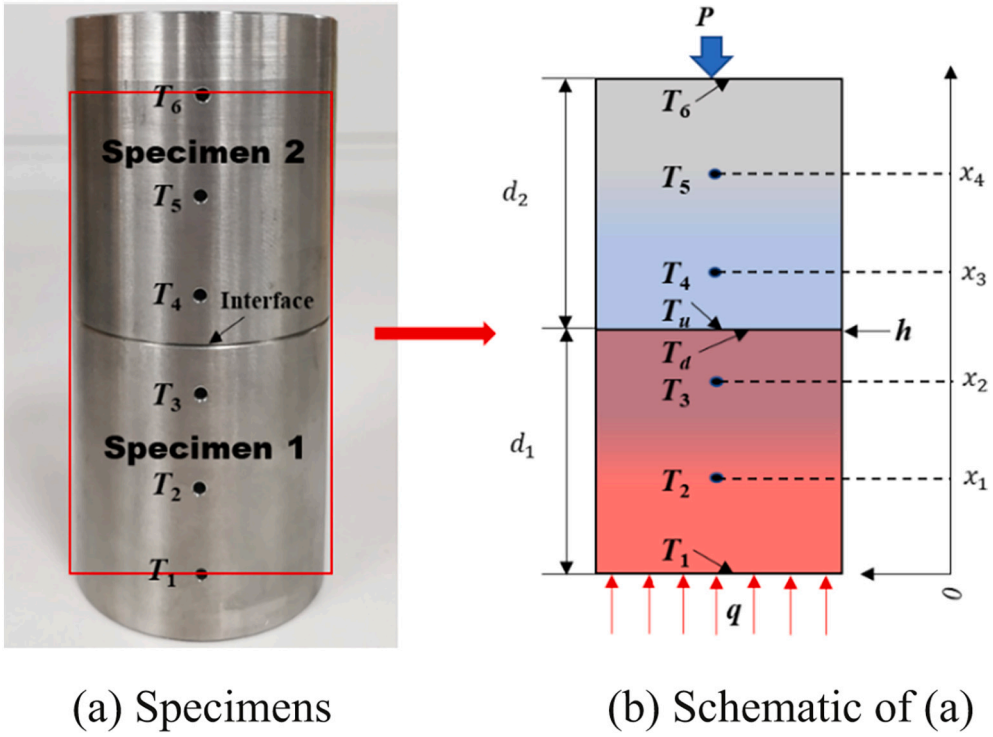

Fig. 4. Two contact specimens and its schematic.

We select the interior region of the red rectangle in Fig.4 (a) and show it in Fig.4 (b). In Fig.4 (b), let T_1 be boundary temperature; let thermal contact conductance be h, axial heat flux be q. With three boundary conditions (T_1, h, q), the 1D heat conduction in Fig.4 (b) has a unique solution, and the solutions are shown in Eqs. (1)–(2),

$$T^{(1)} = -\frac{q}{\lambda_1}x + T_1 \tag{1}$$

$$T^{(2)} = -\frac{q}{\lambda_2}x + T_1 + q\left(\frac{d_1}{\lambda_2} - \frac{1}{h} - \frac{d_1}{\lambda_1}\right) \tag{2}$$

Where $T^{(1)}$ represents the temperature solution of specimen 1, and $T^{(2)}$ is the temperature solution of specimen 2. λ_1 and λ_2 are thermal conductivities of specimen 1 and 2, respectively. Thus, T_2, T_3 and T_d can be calculated with Eqs. (3)–(5),

$$T_2 = -\frac{q}{\lambda_1}x_1 + T_1 \tag{3}$$

$$T_3 = -\frac{q}{\lambda_1}x_2 + T_1 \tag{4}$$

$$T_d = -\frac{q}{\lambda_1}d_1 + T_1 \tag{5}$$

In a similar way, T_u, T_4, T_5 and T_6 can be calculated with Eqs. (6)–(9),

$$T_u = -\frac{q}{\lambda_1}d_1 + T_1 - \frac{q}{h} \tag{6}$$

$$T_4 = -\frac{q}{\lambda_2}x_3 + T_1 + q\left(\frac{d_1}{\lambda_2} - \frac{1}{h} - \frac{d_1}{\lambda_1}\right) \tag{7}$$

$$T_5 = -\frac{q}{\lambda_2}x_4 + T_1 + q\left(\frac{d_1}{\lambda_2} - \frac{1}{h} - \frac{d_1}{\lambda_1}\right) \tag{8}$$

$$T_6 = -\frac{q}{\lambda_2}d_2 + T_1 - q\left(\frac{1}{h} + \frac{d_1}{\lambda_1}\right) \tag{9}$$

Where T_d and T_u are temperatures of two contact surfaces. Note that λ_1 and λ_2 are average thermal conductivity of specimen 1 and 2, respectively. Because d_1 and d_2 are both 40 mm, using average thermal conductivity to calculate temperature distribution is reasonable within d_1 and d_2.

3.3. The treatment for h

TCC can be influenced by temperature and loading pressure, thus, h should also consider the effects of temperature and loading pressure. In many previous studies, researchers often use an empirical fitting correlation to express TCC, as Eq. (10) shows,

$$h = c_1\left(\frac{T_{ave}}{T_r}\right)^{c_2}\left(\frac{P}{E_{eff}}\right)^{c_3} \tag{10}$$

Where P is the loading pressure. T_r is 298 K. T_{ave} is the average temperature of two contact surfaces, namely $T_{ave} = 0.5 * (T_d + T_u)$. E_{eff} is the effective elastic modulus of two contact bodies and can be calculated with Eq. (11),

$$\frac{1}{E_{eff}} = \frac{1-\nu_1^2}{E_1} + \frac{1-\nu_2^2}{E_2} \tag{11}$$

Where E_1 and E_2 are elastic modulus of specimen 1 and 2, respectively. ν_1 and ν_2 are Poisson's ratio of specimen 1 and 2, respectively. According to [19,32], TCC obtained from Eq. (10) is satisfactory within a large temperature and pressure ranges, thus we also use Eq. (10) to calculate TCC. On the other hand, the parameters (c_1, c_2, c_3) in Eq. (10) considers the effects of temperature and pressure on TCC.

3.4. Training data

Generally, training data of ANN is from experiments, however, numerical simulation results can also be training data in some research [29,33]. In this paper, training data is generated using Eqs. (3)–(10), and the detailed descriptions are as follows,

(1) Let q, T_1, λ_1, λ_2, c_1, c_2, c_3, P be independent variables, and h, T_2, T_3, T_d, T_u, T_4, T_5, T_6 be dependent variables.
(2) According to experimental apparatus and material type, give a reasonable value range for each independent variable. The value ranges of all independent variables are listed in Table 3. Note that all the value ranges are reasonable estimation ranges and include all possible experimental conditions.

(3) Assign each independent variable a value from its value range, and then use the independent variable to calculate dependent variables according to Eqs. (3)–(10).
(4) Repeat step (3) many times, thus we can obtain enough training data, and these data is also the solutions of Eqs. (1)–(2).

It should be mentioned that the random combination of c_1, c_2, c_3, P may yield awfully unreasonable h according to Eq. (10), and such data are noisy data, so we let h be in the range of (100,10,000) ($W{\cdot}K^{-1}{\cdot}m^{-2}$). According to the published papers, this range contains TCC values of most of engineering materials with different surface roughness. Besides, T_1 and q should be positively related, and λ_1 is always larger than λ_2 because average temperature of specimen 1 is larger than that of specimen 2. The above rules can be realized by adding additional conditions in the code.

It should be noted that experimental data have some uncertainty. In this paper, we use experimental data to retrieve TCC, so the uncertainty of the experimental data should be considered. For a designed ANN, the common method to enhance its performance or generalization ability is to add noise to training data. In order to make the model consider the uncertainty of actual measurement data, the training data are added by some random noise. Here the random noise can be treated as the uncertainty of the measurement data. We use $T' = T \pm r\,(-3\sigma < r < 3\sigma)$ to add noise to training data. Here r is generated by sampling random numbers from the defined Gaussian distribution with mean μ as zero and standard deviation σ equal to the temperature measurement error 0.75% T, because the main uncertainty comes from the temperature measurement, and temperature measurement error of thermocouples is ±0.75% T in our experimental system. Finally, we obtain 24,048 sets of training data and 6012 sets of test data. Besides, we use the training data without noise and with noise to train the ANN, and we find that the retrieved results of the ANN with noise have a better agreement with the experimental results.

It should also be mentioned that the independent variables can also be assumed to other ranges different from Table 3, that is to say, the method proposed in this paper can also be used to retrieve TCC of other materials.

3.5. The architecture of the designed ANN

The schematic of the designed ANN is shown in Fig.5. The ANN has 1 hidden layer, 1 input layer and 1 output layer. The neuron numbers of the input layer and the output layer are 7 and 6, respectively, however, the neuron number of the hidden layer needs to be determined in the training process.

It can be seen from Fig.5 that we select P, T_1, T_2, T_3, T_4, T_5, T_6 as input data, and q, λ_1, λ_2, c_1, c_2, c_3 as output data. It is because when we finish the training of the ANN model, we can easily use the measured P, T_1, T_2, T_3, T_4, T_5, T_6 from experiment as inputs, and the outputs are q, λ_1, λ_2, c_1, c_2, c_3. Thus, we can simultaneously obtain TCC, heat flux, thermal conductivity of the specimens according to the measured loading pressures and temperatures.

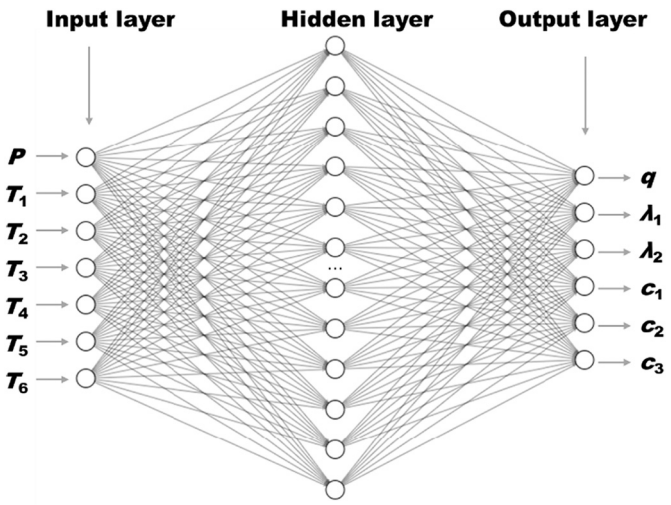

Fig. 5. The architecture of the designed ANN.

We use *Mini-Batch Gradient Descent Algorithm* to train the ANN, and use *Mean Square Error* (*MSE*) to be loss function, as shown in Eq. (12),

$$MSE = \frac{1}{2n}\sum_{i=1}^{n}(y_i - t_i)^2 \tag{12}$$

Where n is the number of output neuron. y_i is the output value, and t_i is the target value. When *MSE* is less than a small value, the ANN finishes training. Furthermore, we use L_2 *Regularization* technique to reduce the effect of overfitting and apply *Min*-max *Normalization Function* to process input data, as shown in Eq. (13),

$$X = \frac{x - x_{\min}}{x_{\max} - x_{\min}} \tag{13}$$

Where $x_{\max}$ and $x_{\min}$ are the maximum and minimum of characteristic value. By Eq. (13), the characteristic value can be transformed to (0,1), which can speed up the training process.

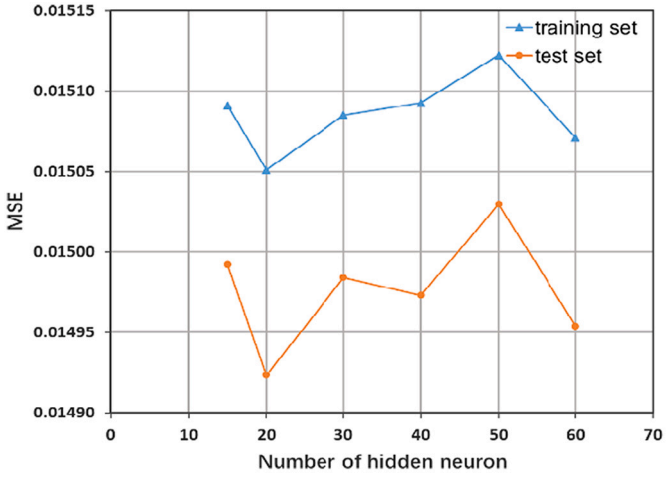

Fig. 6. The performance of ANN with different hidden neurons.

Table 3
The value range of independent variables.

q	T_1	λ_1, λ_2	c_1	c_2	c_3	P
[6000,76,000]	[200,800]	[6,15]	[3000,100,000]	[0.1,3]	[0.1,2]	[0.5,13]

3.6. The number of hidden neurons

Fig.6 shows the performance of the designed ANN with different hidden neurons. It can be seen that the ANN with 20 hidden neurons performs better than others. Therefore, an ANN with 20 hidden neurons is chosen for all next calculations.

Fig.7 shows the training process and the training parameters of the ANN. It can be seen that *MSE* values converge within 2000 epoch training, and overfitting doesn't occur. The training is timesaving and can finish in a PC within 1 h using Python code.

When we finish the ANN training, we can use the experimental P, T_1, T_2, T_3, T_4, T_5, T_6 as input to query the corresponding outputs q, λ_1, λ_2, c_1, c_2, c_3, and the flowchart is shown in Fig.8. Thus, the designed ANN can retrieve q, λ_1, λ_2, c_1, c_2, c_3 simultaneously only based on the experimental P, T_1, T_2, T_3, T_4, T_5, T_6.

4. Results and discussions

4.1. Thermal conductivity λ

We use TC4 titanium alloy to validate our model, and its experimental thermal conductivities can be found in the published papers and are used to validate our retrieved results. Table 4 and Table 5 list the retrieved and experimental thermal conductivities of Pair A and Pair B, respectively. The subscripts "ANN" and "exp" mean the retrieved value by ANN and experimental value, respectively. Δ is the deviation between the retrieved value and the experimental value. It can be seen from Tables 4 and 5 that the deviations are all within 14%, and deviations of 95% cases are less than 10%, besides, the deviations of 66.7% case are less than 5%.

ASTM E1225–13 pointed out that the deviation should be less than 18% for thermal conductivity measurement in different labs. Although retrieved thermal conductivity is obtained by ANN rather than experiments, it can also say that our results are in accordance with the standard. Guo et al. [34] used conjugate gradient method to estimate the thermal conductivity and TCC of one layer in a multilayer composite structure. The results of a heat-shielding experiment showed no more than a 2.4% deviation for the estimated thermal conductivity. However, their research neglected TCC between other interfaces and thermal conductivity of other layers were known. Considering the difference in experimental apparatus, their research can also be a support for our research.

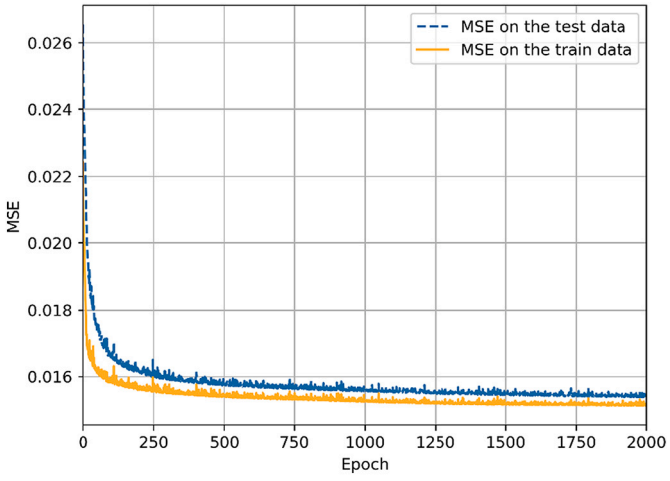

Fig. 7. Training process (Learning rate = 0.15, Epoch = 2000, Mini-Batch = 10, Regularization parameter = 1.0).

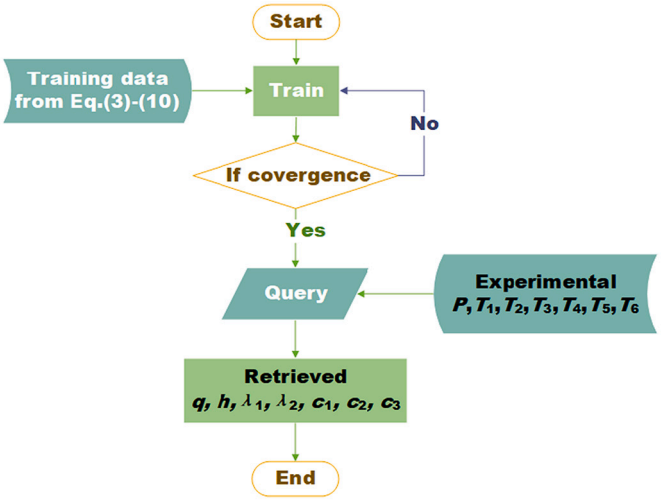

Fig. 8. The flowchart for retrieving TCC.

4.2. Heat flux q

Tables 6 and 7 list the retrieved heat flux q_{ANN} and the experimental heat flux q_{exp}, and q_{exp} is calculated with Fourier's law of heat conduction. It can be seen that the deviations at 400 °C are relatively larger than that at other heating temperatures, which may be caused by the system error at 400 °C. The retrieved heat flux at other heating temperatures (500 °C, 600 °C, 700 °C) agrees well with the experimental heat flux, and the maximum deviation is 5.4%, which also shows that the ANN model performs well.

4.3. c_1, c_2, c_3

Table 8 lists the retrieved c_1, c_2, c_3 for determining TCC h. It can be seen that c_1 of Pair A is slightly different from that of Pair B, and we think it is due to numerical error during normalization process, thus, we conclude that c_1 is the same for the same material pairs even though their surface roughness is different. In addition, c_2 is 1.55 for both Pair A and B. It is reasonable because c_2 is the exponent of temperature term in Eq. (10), and it can be concluded that the effect of temperature on TCC of the same material pairs should be the same even though their surface roughness is different.

It can also be seen from Table 8 that c_3 is different for two contact pairs. It is well known to us that surface roughness can strongly affect TCC, because different surface roughness can contribute to different actual contact area. It can be inferred when other conditions keep the same, if we apply the same pressure to two contact pairs with different surface roughness, TCC of different pairs must be different. In our study, c_3 is the exponent of pressure term in Eq. (10), and the results for two contact pairs agree well with the inference. Besides, the term P/E_{eff} in Eq. (10) is always less than 1.0 in most cases, hence, the bigger the exponent of P/E_{eff} in Eq. (10), the smaller the TCC. In our study, the surface roughness of Pair A is less than that of Pair B, so it can be inferred that TCC of Pair A is larger than that of Pair B when other conditions keep the same, and the retrieved results are in accordance well with the inference.

Dou et al. [35] studied the effect of roughness on TCC of stainless steel and obtained an empirical fitting correlation similar with Eq.(10). In their results, c_1 and c_2 are largely different for stainless steel pairs with different surface roughness. However, in our study, c_1 and c_2 are the same for the contact pairs with different surface roughness. According to our results, we think c_1 is related to material type; c_2 is related to temperature; c_3 is related to pressure and surface roughness. Such a conclusion is clear, reasonable and easier to understand.

Table 4
The retrieved and experimental thermal conductivities of Pair A.

4.65 MPa				7.78 MPa				12.08 MPa			
T/°C	λ_{ANN}	λ_{exp}	Δ	T/°C	λ_{ANN}	λ_{exp}	Δ	T/°C	λ_{ANN}	λ_{exp}	Δ
174.7	7.5	8.3	−9.6%	175.3	7.4	8.3	−10.8%	172.7	7.2	8.3	−13.3%
217.5	8.9	8.8	1.1%	218.4	8.7	8.8	−1.1%	217.5	8.6	8.8	−2.3%
263.2	9.8	9.2	6.5%	263.0	9.6	9.2	4.3%	260.5	9.3	9.2	1.1%
306.4	10.4	9.7	7.2%	306.9	10.1	9.7	4.1%	305.5	9.9	9.7	2.1%
377.1	10.5	10.3	1.9%	383.0	10.5	10.4	1.0%	386.5	10.3	10.4	−1.0%
453.4	11.8	11.1	6.3%	458.6	11.7	11.2	4.5%	461.1	11.5	11.2	2.7%
525.2	12.7	11.8	7.6%	531.9	12.6	11.9	5.9%	536.2	12.4	11.9	4.2%

Table 5
The retrieved and experimental thermal conductivities of Pair B.

T/°C	4.65 MPa			7.78 MPa			12.08 MPa		
	λ_{ANN}	λ_{exp}	Δ	λ_{ANN}	λ_{exp}	Δ	λ_{ANN}	λ_{exp}	Δ
157.8	7.0	7.5	−6.7%	7.0	7.5	−6.7%	6.9	7.5	−8.0%
197.4	7.9	7.7	2.6%	7.8	7.7	1.3%	7.8	7.7	1.3%
238.1	8.4	7.9	6.3%	8.3	7.9	5.1%	8.2	7.9	3.8%
279.8	8.8	8.2	7.3%	8.6	8.2	4.9%	8.3	8.1	2.5%
341.0	9.6	10.0	−4.0%	9.6	10.0	−4.0%	9.6	10.0	−4.0%
410.1	10.9	10.7	1.9%	10.8	10.7	0.9%	10.6	10.7	−0.9%
478.0	11.8	11.4	3.5%	11.6	11.4	1.8%	11.5	11.4	0.9%

Table 6
The retrieved and experimental heat flux of Pair A.

4.65 MPa				7.78 MPa			12.08 MPa		
Heating Temperature	q_{ANN}	q_{exp}	Δ	q_{ANN}	q_{exp}	Δ	q_{ANN}	q_{exp}	Δ
400 °C	16,999.5	19,492.8	−12.8%	17,597.0	20,459.2	−14.0%	17,550.0	21,096.3	−16.8%
500 °C	25,874.9	26,313.8	−1.7%	26,593.0	27,583.1	−3.6%	26,922.1	28,468.4	−5.4%
600 °C	34,375.6	33,753.6	1.8%	34,987.9	35,177.8	−0.5%	35,205.0	36,281.9	−3.0%
700 °C	42,270.8	41,504.7	1.8%	43,045.7	43,296.1	−0.6%	43,479.2	44,787.7	−2.9%

Table 7
The retrieved and experimental heat flux of Pair B.

4.65 MPa				7.78 MPa			12.08 MPa		
Heating Temperature	q_{ANN}	q_{exp}	Δ	q_{ANN}	q_{exp}	Δ	q_{ANN}	q_{exp}	Δ
400 °C	19,573.3	22,864.0	−12.8%	20,272.6	23,681.3	−13.2%	20,390.6	24,088.2	−14.6%
500 °C	29,387.8	30,563.8	−3.0%	30,031.3	31,615.1	−4.3%	30,237.4	32,130.6	−5.4%
600 °C	38,893.2	38,867.3	−0.2%	39,367.0	40,002.5	−1.8%	39,453.4	40,725.5	−3.6%
700 °C	48,297.8	47,692.9	0.4%	48,824.7	49,084.5	−1.4%	49,246.5	50,482.1	−3.8%

Table 8
The retrieved c_1, c_2, c_3.

Contact pair	c_1/W·K^{-1}·m^{-2}	c_2	c_3
Pair A	52,489.6	1.55	0.37
Pair B	51,635.4	1.55	0.44

4.4. TCC h

Table 9 and Table 10 list the retrieved and experimental TCC of Pair A and Pair B, respectively. It can be seen that the deviation between h_{ANN} and h_{exp} fluctuates with average interface temperatures and pressures. Specifically, the maximum deviation is 42.1% and minimum deviation is 1.2%.

However, it should be emphasized that h_{exp} is an indirect measurement value, so measurement errors can't be avoided. As stated in Section 1, extrapolation method and linear fitting method may yield

Table 9
The retrieved and experimental TCC of Pair A.

4.65 MPa				7.78 MPa				12.08 MPa			
T_{ave}/°C	h_{ANN}	h_{exp}	Δ	T_{ave}/°C	h_{ANN}	h_{exp}	Δ	T_{ave}/°C	h_{ANN}	h_{exp}	Δ
216.7	3573.4	3215.4	11.1%	218.9	4355.2	3472.2	25.4%	217.4	5099.6	3787.9	34.6%
270.5	4245.2	3968.3	7.0%	273.5	5183.0	4081.6	27.0%	274.1	6110.6	4651.2	31.4%
327.1	5007.1	4717.0	6.1%	329.0	6090.2	4975.1	22.4%	328.2	7151.3	5814.0	23.0%
380.5	5778.9	5555.6	4.0%	383.6	7047.8	5780.3	21.9%	384.3	8308.8	6896.6	20.5%

Table 10
The retrieved and experimental TCC of Pair B.

4.65 MPa				7.78 MPa				12.08 MPa			
T_{ave}/°C	h_{ANN}	h_{exp}	Δ	T_{ave}/°C	h_{ANN}	h_{exp}	Δ	T_{ave}/°C	h_{ANN}	h_{exp}	Δ
215.1	1851.5	2293.6	−19.3%	219.6	2357.7	3533.6	−33.3%	220.0	2865.2	4950.5	−42.1%
271.4	2222.6	2403.8	−7.5%	275.2	2820.2	3344.5	−15.7%	276.8	3439.5	4347.8	−20.9%
330.4	2645.1	2427.2	9.0%	332.8	3339.8	3246.8	2.9%	331.9	4043.1	4566.2	−11.5%
387.4	3086.6	2717.4	13.6%	389.6	3893.3	3846.2	1.2%	390.1	4732.2	7633.6	−38.0%

significantly different results for the same experimental data. The detailed uncertainty analysis about our measurement system can be found in [9]. According to [9], the relative experimental uncertainty for Pair A is 14.1%–19.0%, and for Pair B is 5.8%–7.3%. Besides, the relative experimental uncertainty increases with an increase in loading pressure, because a higher loading pressure will reduce the thermal contact resistance, thus the relative uncertainty will increase. Hence, h_{exp} calculated by linear fitting method in air condition is only a relatively reliable value, and we think it may be one of the causes of the large deviations in some cases.

On the other hand, whether numerical model or ANN model, both of them are constructed based on some assumptions, which is also another cause of the large deviations in some cases. Besides, it should be noted that the TCC is the data-reduction result related to thermal conductivity, temperature and heat flux, so the uncertainty of TCC will be enlarged step by step in the data-reduction process. In our retrieved results, the deviations of the thermal conductivity and heat flux are obviously smaller than that of TCC. Thus, the accumulation of uncertainties may be another reason for some relatively large uncertainties in some retrieved TCC.

In a word, although deviations in some cases are relatively large, we still consider that our method is believable. The reasons are as follows:

(1) Firstly, the retrieved thermal conductivities and heat flux agree well with the experimental values.
(2) Secondly, the deviations of 50% cases are less than 20% for the retrieved TCC, and such a result is completely acceptable for TCC prediction.
(3) Thirdly, the retrieved c_1, c_2 and c_3 are reasonable and can be explained conceptually.

5. Conclusions

In this paper, we design an artificial neural network (ANN) model to retrieve thermal contact conductance (TCC) only based on the measured temperatures and loading pressures, besides, thermal conductivity and heat flux of the specimens can be retrieved simultaneously. The method can omit the measurement of heat flux and thermal conductivities of the specimens, and the whole computation process can be finished within 1 h. The major conclusions are as follows:

(1) The retrieved thermal conductivities and heat flux by ANN model agree well with the experimental values. The deviations between the retrieved and experimental TCC of 50% cases are less than 20%.
(2) The ANN model can consider the effects of temperature, loading pressure and surface roughness on TCC. If we use $h = c_1\left(\frac{T_{ave}}{T_r}\right)^{c_2}\left(\frac{P}{E_{eff}}\right)^{c_3}$ to be the empirical fitting correlation of TCC, the retrieved c_1 and c_2 are the same for the same material pairs even though the surface roughness is different, and c_3 is different for contact pairs with different surface roughness.
(3) According to our results, it is believed that c_1 is related to material type; c_2 is related to temperature; c_3 is related to pressure and surface roughness. Such a conclusion is more clear, reasonable and easier to understand.

CRediT authorship contribution statement

Xing-Jie Ren: Conceptualization, Investigation, Methodology, Writing – original draft, Writing – review & editing. **Jian-Jun Gou:** Writing – original draft, Investigation. **Yan-Jun Dai:** Writing – original draft, Funding acquisition. **Wen-Quan Tao:** Conceptualization, Writing – original draft, Writing – review & editing, Funding acquisition, Supervision.

Declaration of Competing Interest

None.

Acknowledgement

This study is supported by the NNSFC (51836005), the Foundation for Innovative Research Groups of the National Natural Science Foundation of China (No.51721004), and the 111 project (B16038).

References

[1] R.R. Kumar, R. Palaninathan, E. Kishor, et al., Role of thermal contact conductance on sandwich-type metallic thermal protection system profile, AIAA J. 50 (10) (2012) 2194–2201.
[2] X. Wang, H. Li, R. Yao, et al., Thermal contact resistance optimization of press-pack IGBT device based on liquid metal thermal interface material, IEEE Trans. Power Electron. (2021) 5411–5421.
[3] S.C. Indrakanti, J.-G. Kim, C.H. Kim, et al., Application of thermal network models for analysis and design of superconducting cable components, IEEE Trans. Appl. Supercond. 27 (4) (2017) 1–5.
[4] Z. Yang, Y. Yang, J. Liang, et al., An analysis method of thermal interface of cryogenic cooling path, IEEE Trans. Appl. Supercond. 29 (2) (2019) 1–2.
[5] M. Alsayed, B. Manshoor, H. Salleh, Measurement of heat flow for contact resistance and thermal conductivity in fuel cell material, J. Complex Flow 1 (2) (2019).
[6] D. Taler, P. Ocłoń, Thermal contact resistance in plate fin-and-tube heat exchangers, determined by experimental data and CFD simulations, Int. J. Therm. Sci. 84 (2014) 309–322.
[7] P. Zhang, T. Cui, Q. Li, Effect of surface roughness on thermal contact resistance of aluminium alloy, Appl. Therm. Eng. 121 (2017) 992–998.
[8] V. Gopal, M.J. Whiting, J.W. Chew, et al., Thermal contact conductance and its dependence on load cycling, Int. J. Heat Mass Transf. 66 (2013) 444–450.
[9] X.J. Ren, H. Ding, Y.J. Dai, et al., Experimental study on thermal contact resistance of carbon fiber reinforced silicon carbide composite with 3D needled preform (3DN C/SiC), Int. Commun. Heat Mass Transf. 124 (2021), 105271.
[10] T. Kim, S. Kim, E. Kim, et al., High-temperature skin softening materials overcoming the trade-off between thermal conductivity and thermal contact resistance, Small 17 (38) (2021) 2102128.
[11] R. Joseph, N.A. Kumar, S.S. Kumar, Effect of interstitial compounds in controlling thermal contact conductance across pressed joints at cryogenic temperature and low contact pressure, Appl. Therm. Eng. 194 (2021), 117073.
[12] M.M. Yovanovich, Four decades of research on thermal contact, gap, and joint resistance in microelectronics, Ieee Trans. Components Packaging Technol. 28 (2) (2005) 182–206.
[13] S.Y. Mesnyankin, A.G. Vikulov, D.G. Vikulov, Solid-solid thermal contact problems: current understanding, Physics-Uspekhi 52 (9) (2009) 891–914.
[14] X. Zhang, P.Z. Cong, M. Fujii, A study on thermal contact resistance at the interface of two solids, Int. J. Thermophys. 27 (3) (2006) 880–895.
[15] P. Sadowski, S. Stupkiewicz, A model of thermal contact conductance at high real contact area fractions, Wear 268 (1–2) (2010) 77–85.
[16] Y. Frekers, T. Helmig, E.M. Burghold, et al., A numerical approach for investigating thermal contact conductance, Int. J. Therm. Sci. 121 (2017) 45–54.
[17] J.L. Liu, C. Ma, S.L. Wang, et al., Thermal contact resistance between bearing inner ring and shaft journal, Int. J. Therm. Sci. 138 (2019) 521–535.
[18] J.J. Gou, X.J. Ren, Y.J. Dai, et al., Study of thermal contact resistance of rough surfaces based on the practical topography, Comput. Fluids 164 (2018) 2–11.

[19] X.J. Ren, Y.J. Dai, J.J. Gou, et al., Numerical study on thermal contact resistance of 8-harness satin woven pierced composite, Int. J. Therm. Sci. 159 (2021), 106584.
[20] M. Chen, Q. Li, P. Zhang, Numerical prediction of high temperature thermal contact resistance of HTA–C/ZrB2-SiC with radiation effects, Int. Commun. Heat Mass Transf. 120 (2021), 105058.
[21] Y. Frekers, S. Vieler, S. van Buren, et al., Determination of thermal contact resistance coefficients through thermo-mechanical simulation, in: International Heat Transfer Conference Digital Library, Begel House Inc., 2014.
[22] ASTM, Standard Test Method for Thermal Conductivity of Solids using the Guarded-Comparative-Longitudinal Heat Flow Technique, ASTM International, West Conshohocken, PA, 2013, pp. 1–10.
[23] D.H. Liu, Y. Luo, X.C. Shang, Experimental investigation of high temperature thermal contact resistance between high thermal conductivity C/C material and inconel 600, Int. J. Heat Mass Transf. 80 (2015) 407–410.
[24] T.R. Thomas, Extrapolation errors in thermal contact resistance measurements, ASME J. Heat Transf. 97 (2) (1975) 305–307.
[25] T. Roy, Fitting a straight-line when both variables are subject to error - pharmaceutical applications, J. Pharm. Biomed. Anal. 12 (10) (1994) 1265–1269.
[26] A.E. Stark, Thermal Contact Resistance Measurement and Related Uncertainties, Old Dominion University, Norfolk, 2020.
[27] K. Goudarzi, A. Moosaie, M. Gharaati, Applying artificial neural networks (ANN) to the estimation of thermal contact conductance in the exhaust valve of internal combustion engine, Appl. Therm. Eng. 87 (2015) 688–697.
[28] T. Zhan, L. Fang, Y. Xu, Prediction of thermal boundary resistance by the machine learning method, Sci. Rep. 7 (1) (2017) 7109.
[29] H. Yang, Z. Zhang, J. Zhang, et al., Machine learning and artificial neural network prediction of interfacial thermal resistance between graphene and hexagonal boron nitride, Nanoscale 10 (40) (2018) 19092–19099.
[30] E.M. Burghold, Y. Frekers, R. Kneer, Transient contact heat transfer measurements based on high-speed IR-thermography, Int. J. Therm. Sci. 115 (2017) 169–175.
[31] M.A. Nielsen, Neural networks and deep learning. Vol. 25., San Francisco, Determination press, CA, 2015.
[32] Y.J. Dai, J.J. Gou, X.J. Ren, et al., A test-validated prediction model of thermal contact resistance for Ti-6Al-4V alloy, Appl. Energy 228 (2018) 1601–1617.
[33] H. Wu, W.-Z. Fang, Q. Kang, et al., Predicting effective diffusivity of porous media from images by deep learning, Sci. Rep. 9 (1) (2019) 20387.
[34] J. Guo, X. Chen, Z. Qu, et al., Reverse identification method for simultaneous estimation of thermal conductivity and thermal contact conductance of multilayered composites, Int. J. Heat Mass Transf. 173 (2021), 121244.
[35] R. Dou, T. Ge, X. Liu, et al., Effects of contact pressure, interface temperature, and surface roughness on thermal contact conductance between stainless steel surfaces under atmosphere condition, Int. J. Heat Mass Transf. 94 (2016) 156–163.